

Comparative high-pressure structural and electrical transport properties study of thermoelectric $(\text{Bi}_{1-x}\text{Sb}_x)_2\text{Te}_3$ compounds

Chenxin Wei^{1,2}, Dawod Muhamed², Wenting Lu^{1,2}, Haikai Zou^{1,2},
 Baihong Sun^{1,2}, Shiyu Feng^{1,2}, Qian Zhang¹, Zegeng Su²,
 Hirokazu Kadobayashi³, Martin Kunz⁴, Bihang Wang⁵,
 Azkar, Saeed Ahmad^{1,6}, Yaron Amouya^{2*}, Elissaios Stavrou^{1,2,6*}

¹Materials Science and Engineering Department, Guangdong Technion-Israel Institute of Technology, Shantou, 515063, China.

²Department of Materials Science and Engineering, Technion-Israel Institute of Technology, Haifa, 3200003, Israel.

³Spring-8/JASRI, 1-1-1 Kouto, Sayo-gun, Hyogo 679-5198, Japan.

⁴Advanced Light Source, Lawrence Berkeley National Laboratory, Berkeley, 94720, California, USA.

⁵Deutsches Elektronen-Synchrotron, DESY, Hamburg, D-22603, Germany.

⁶Guangdong Provincial Key Laboratory of Materials and Technologies for Energy Conversion, Guangdong Technion-Israel Institute of Technology, Shantou, 515063, State, China.

*Corresponding author(s). E-mail(s): amouyal@technion.ac.il;
elissaios.stavrou@gtiit.edu.cn;

Abstract

Thermoelectric $(\text{Bi}_{1-x}\text{Sb}_x)_2\text{Te}_3$ (BST-x) compounds with $x=0.2, 0.7$ and 0.9 have been studied using synchrotron angle-dispersive powder x-ray diffraction in a diamond anvil cell up to 25 GPa (at room temperature). The results clearly indicate that all compounds of this study follow a similar structural evolution with the one of pure Bi_2Te_3 and Sb_2Te_3 under pressure. From the comparison between the critical pressures of the corresponding phase transitions, a clear trend of increasing critical pressure for the transition to the disordered solid-solution BCC phase was observed with the increase of Sb concentration. In the case of the

BST-0.7, an extended stability of the solid-solution BCC phase up to, at least, 180 GPa was observed. Finally, electrical transport properties measurements under pressure for BST-0.7, document a reversible pressure-induced metallization above 12 GPa.

Keywords: High-pressure, Thermoelectric materials, X-ray diffraction, electrical properties

1 Introduction

$\text{Bi}_2\text{Te}_3\text{-Sb}_2\text{Te}_3$ compounds ($(\text{Bi}_{1-x}\text{Sb}_x)_2\text{Te}_3$, BST- x) have been extensively studied due to their outstanding thermoelectric properties at near-room temperature ranging from 300-500K [1–4]. The BST- x system exhibits full solubility. At ambient conditions, Bi_2Te_3 , Sb_2Te_3 and BST compounds adopt the rhombohedral tetradymite crystal structure (space group $R-3m$ (166)), formed by monoatomic sublayers of Bi/Sb, and Te atoms [5–7], independently of the relative concentration of Bi and Sb. The quintuple layers of Te-Bi(Sb)-Te-Bi(Sb)-Te are stacked in a sequence along c -axis direction [8, 9].

The high-pressure studies of Bi_2Te_3 and Sb_2Te_3 end members were motivated mainly by the possibility of using pressure to improve their higher thermoelectric conversion efficiency [10–12] and the increasing interest of the superconducting phase [13–16]. Bi_2Te_3 and Sb_2Te_3 , exhibit, at least, three phase transitions under pressure. Zhu *et al.* [17] clarified that Bi_2Te_3 transforms from the rhombohedral $R-3m$ (six-fold) phase ($\alpha\text{-Bi}_2\text{Te}_3$ or phase I) to a monoclinic $C2/m$ (seven-fold) phase at 8 GPa ($\beta\text{-Bi}_2\text{Te}_3$ or phase II) and then to a $C2/c$ (eight-fold) phase at 14 GPa ($\gamma\text{-Bi}_2\text{Te}_3$ or phase III). At higher pressures, Bi_2Te_3 adopts a disorder solid-solution body-center cubic (BCC, A2) $Im-3m$ structure (phase IV), with a 40% and 60% occupancy of the 2a Wyckoff Position (WP) for Bi and Te atoms, respectively [17, 18]. Identical structural evolution was concluded for Sb_2Te_3 [19, 20], albeit with slightly different critical pressures. It is noteworthy, that the disordered BCC structure for Sb_2Te_3 appears at pressure above 20 GPa [19].

Studies on the structural evolution of $\text{Bi}_{1-x}\text{Sb}_x\text{Te}_3$ compounds under pressure are extremely limited. Indeed, Bai *et al.* [21] studied $\text{Bi}_{0.5}\text{Sb}_{1.5}\text{Te}_3$ (BST-0.75) only inside the pressure stability range of the ambient phase, <10 GPa. Jacobsen *et al.* [5], studied BiSbTe_3 (BST-0.5) up to 18 GPa, and a phase transition was observed at \approx 7 GPa. However, the indexing of the high-pressure phase was not the one concluded by more recent studies on Bi_2Te_3 and Sb_2Te_3 .

Motivated by the above, we have performed a detailed comparative *in-situ* synchrotron angle-dispersive powder x-ray diffraction (ADXRD) study of three different BST- x compounds with $x=0.2, 0.7$ and 0.9 , up to 20+ GPa. Our main motivation was to explore the structural evolution under pressure as a function of varying Sb concentration. Our results document that the three BST compounds follow the same phase sequence with the pure Bi_2Te_3 and Sb_2Te_3 under pressure, without any noticeable

effect of the Sb concentration on the critical pressures for the first two phase transitions. On the other hand, it is apparent that the increase of the Sb concentration results to an increase of the critical pressure for the formation of the BCC phase.

In the case of BST-0.7, our study was extended to ≈ 180 GPa, with the aim of exploring the stability of the BCC phase under Mbar pressures. Surprisingly, we observe that the BCC solid-solution phase remains stable up to the highest pressure of this study. Finally, for the same BST-0.7, *in-situ* electrical transport measurements as a function of pressure and temperature were performed. A clear indication for metallization was observed above ≈ 12 GPa.

2 Experimental methods

2.1 Material Synthesis

$(\text{Bi}_{1-x}\text{Sb}_x)_2\text{Te}_3$ (BST- x) specimens with $x = 0.2, 0.7$ and 0.9 were synthesized by mixing commercial high-purity Bi, Sb and Te chunks (Alfa Aesar; 99.999 % purity) in quartz tubes according to the appropriate stoichiometric ratio. The tubes were sealed under vacuum (10^{-5} Torr) and annealed at 1123 K for 8.5 h to melt the raw materials, and then cooled down to 300 K during 16 h [4]. The obtained ingots were ground into fine powders and sieved using a 56 μm mesh.

2.2 High pressure studies

A BX-80 type diamond anvil cell (DAC) with 400 μm diameter diamond culets was used for the high-pressure experiments. A Rhenium foil pre-indented to $\approx 50\mu\text{m}$ and a central hole diameter of $\approx 130\mu\text{m}$ with was used as gasket. Samples were loaded near the center of the sample chamber, along with a ruby chip and gold used as pressure markers, at the side. The shift of ruby line [22] and the EOS of gold [23] were used to determine the pressure *in-situ*. Neon (Ne) was used as pressure transmitting medium (PTM) which is capable to maintain hydrostatic environment up to 20 GPa [24], and loaded with a gas loader. For the study of BST-0.7 up to 180 GPa, beveled 100 μm diameter diamond culets were used and a Rhenium foil pre-indented to $\approx 30\mu\text{m}$ with a hole of 40 μm in diameter was used as gasket. Ne was used as the PTM.

2.2.1 X-ray Diffraction

X-ray diffraction (XRD) measurements at ambient conditions were performed with the Cu $K\alpha_1$ ($\lambda=1.540598\text{\AA}$) X-ray line (Rigaku MiniFlex, Tokyo, Japan) to identify the starting crystal structures, see Fig. S1. The results confirm that all BST specimens adopt the rhombohedral tetradymite $R-3m$ crystal structure under ambient conditions, without any trace of impurity.

A Dectris Pilatus3 S 1M Hybrid Photon Counting detector was used at the Advanced Light Source, Lawrence Berkeley National Laboratory, Beamline 12.2.2. The spot size of the X-ray probing beam was focused to about $10 \times 10\mu\text{m}$ using Kirkpatrick-Baez mirrors. More details on the XRD experimental setups are given in Kunz *et al.* [25]. At SPring-8, beamline BL10XU, a Flat Panel X-ray Detector (Varex Imaging,

XRD1611 CP3) was used and the X-ray probing beam spot size was focused to approximately $10 \times 10 \mu\text{m}$ using Kirkpatrick-Baez mirrors. More details on the SPring-8 XRD experimental setups are given in Kawaguchi-Imada *et al.* [26]. At Beamline P02.2 at DESY, the X-ray probing beam were focused to a spot size of $2 \times 2 \mu\text{m}$ at the sample using Kirkpatrick-Baez mirrors and a PerkinElmer XRD 1621 flat-panel detector was used to collect the diffraction images of sample.

The integration of powder diffraction patterns to produce scattering intensity versus 2θ diagrams and initial analysis were performed using the DIOPTAS program [27]. Calculated XRD patterns were produced using the POWDER CELL program [28] for the corresponding crystal structures according to the EOSs determined experimentally in this study and assuming continuous Debye rings of uniform intensity. XRD patterns indexing has been performed using the DICVOL program [29] as implemented in the FullProf Suite. Rietveld refinements were performed using the *GSAS – II* software [30].

2.2.2 Electrical measurements

In-situ high-pressure electrical resistance measurements for BST-0.7 were performed using the standard four-point probe method [R_1, R_2]. A T301 stainless steel gasket was first indented and a hole was drilled with a diameter of $300 \mu\text{m}$. Cubic boron nitride (cBN) insulation powder was used to fill the hole and cover the steel to minimize its influence on the electrical measurement. After compressing cBN to ≈ 20 GPa, a smaller hole was drilled in the center with $\approx 150 \mu\text{m}$ in diameter. The rest of the gasket was covered with an epoxy insulating layer to further protect the electrode leads from the metallic gasket. Four electrodes were cut from a Pt foil and used for the electrical connection with the specimen.

The sample chamber was fully filled with the sample along with a small ruby chip at the center of the anvil for pressure calibration. No PTM was used during the measurement because it would permeate the space between the sample powders and interfere with their intimate contact upon pressing. The sample and the Pt probes were pressurized to about ≈ 2 GPa in the DAC to achieve full electrical contact of the sample with the probes. Ruby powder was used as the pressure marker

3 Results

3.1 X-ray Diffraction

3.1.1 X-ray Diffraction of BST-0.2,0.7 and 0.9 up to 20-25 GPa

XRD patterns of the BST specimens of this study at selected pressures are shown in Figure 1. All BST compounds remain in the rhombohedral phase (phase I) from ambient pressure up to ≈ 8 -10 GPa. Above this pressure, a clear phase transition was observed, based on the gradual appearance and disappearance of Bragg peaks, towards the first high pressure phase (phase II). The coexistence of phase I and phase II is apparent up to 2-3 GPa above the first indication of the appearance of phase II. Above this pressure only the peaks of phase II can be detected. Above ≈ 15 GPa, another phase transition is evident towards the second high-pressure phase, phase III.

As in the case of the Phase I \rightarrow Phase II transition, Phases II and III also coexist for a certain pressure range. However, a clear increase of the pressure range of the coexistence is observed with increasing concentration of Sb. At even higher pressures, new Bragg peaks appear for BST-02 and BST-09, above 17.2 and 23 GPa, respectively; see arrows in Fig. 1(a) and (c). This is attributed to the third high-pressure phase IV that coexists with phase III for BST-0.2 and BST-0.9 up to the highest pressures of this study.

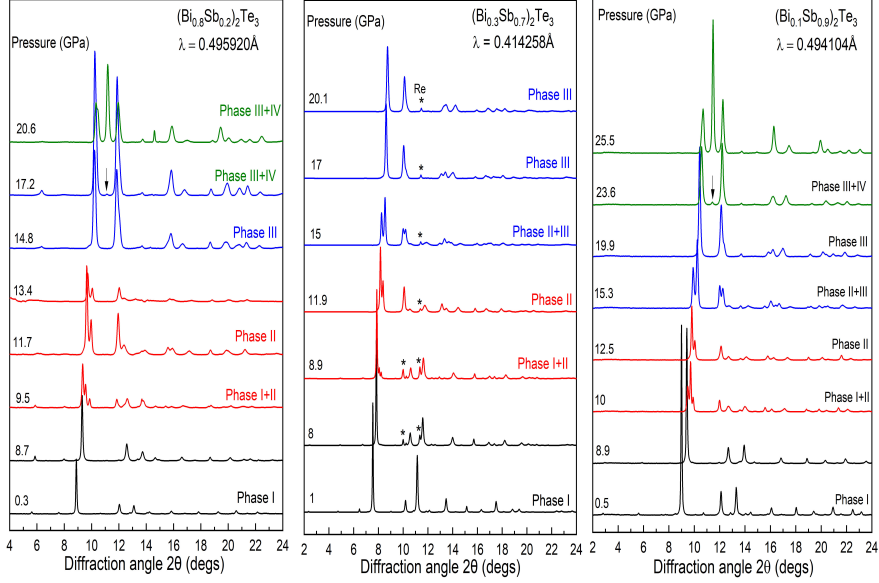


Fig. 1 XRD patterns of (a) BST-0.2, (b) BST-0.7 and (c) BST-0.9 at selected pressures. The peaks marked with asterisks originate from Re gasket material. The relevant predominant phases, Phase I ($R-3m$), Phase II ($C2/m$) and Phase III ($C2/c$) are noted with different colours. The arrows in (a) and (c) denote the first appearance of the strongest peak (110) of the BCC phase (phase IV). The corresponding X-ray wavelengths are noted inside the panels.

A more detailed comparison of the high-pressure phases reveals that all BST specimens adopt identical high-pressure phases: phase II and III; see Fig. S2. Moreover, both phases II and III can be indexed with the previously reported Phase II (space group $C2/m$ (12), $Z=4$) and phase III (space group $C2/c$ (15), $Z=4$) monoclinic phases of Bi_2Te_3 at similar pressures [17]. Thus, we conclude that all the BST specimens of this study qualitatively follow the same structural evolution, including the co-existence of phases pressure ranges, under pressure with Bi_2Te_3 , *i.e.* rhombohedral $R-3m$ (phase I) \rightarrow monoclinic $C2/m$ (phase II) \rightarrow monoclinic $C2/c$ (phase III) \rightarrow disordered BCC (phase IV). The reader is referred to the bar diagram in Fig. 2 for a detailed account of the critical pressures and stability pressure ranges for the observed phase transitions and phases.

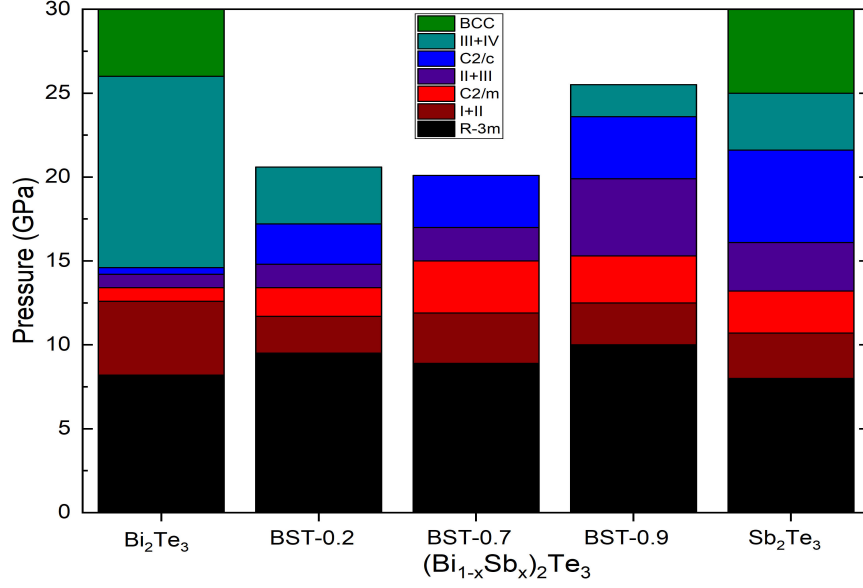


Fig. 2 Bar diagram showing the pressure stability intervals of the different structural modifications (Phase I ($R-3m$), Phase II ($C2/m$), Phase III ($C2/c$) and phase IV ($Im-3m$) of BST compounds and Bi_2Te_3 and Sb_2Te_3 end members. The data for Bi_2Te_3 and Sb_2Te_3 are adopted from Ref. [17] and Ref. [19], respectively.

From the relevant Rietveld refinements of the XRD patterns, see Fig. S3, using the crystal structures mentioned above, the experimental lattice parameters and cell volumes were determined and are plotted as a function of pressure in Fig. 3 and listed in Table 1. From the data of Fig. 3(d)-(f), the bulk modulus B and its pressure derivative B' were determined by fitting a third-order Birch-Murnaghan [31] Equation of State (EOS), Eq. 1, to the experimental data, see Table 1.

$$P = \frac{3}{2}B_{T_0} \left[\left(\frac{V_0}{V} \right)^{\frac{7}{3}} - \left(\frac{V_0}{V} \right)^{\frac{5}{3}} \right] \times \left\{ 1 + \frac{3}{4} (B'_{T_0} - 4) \left[\left(\frac{V_0}{V} \right)^{\frac{2}{3}} - 1 \right] \right\} \quad (1)$$

Table 1 Experimental structural parameters of BST-0.2, 0.7 and 0.9 at selected pressures: space group (SG), number of formula units in the unit cell Z , lattice parameters, cell volume per formula unit V_{pfu} , bulk modulus B and its pressure derivative B' (as determined by fitting a 3^{rd} order Birch-Murnaghan EOS [31] to the experimental data) at the onset pressure.

P (GPa)	SG	Z	a (Å)	b (Å)	c(Å)	V_{pfu} (Å ³)	B (GPa)	B'
BST-0.2								
ambient	R-3m	3	4.359	4.359	30.506	167.316	39(4)	6.0 (0.4)
0.9	R-3m	3	4.351	4.351	30.341	165.797		
10.5	C2/m	4	14.688	4.141	8.958	136.151	79.4 (4.9)	4 (fix)
14.8	C2/c	4	9.991	6.918	7.706	125.471	82.5 (4.6)	4 (fix)
BST-0.7								
ambient	R-3m	3	4.303	4.30	30.430	162.638	22.9 (10)	13.5 (1.1)
3	R-3m	3	4.206	4.206	29.563	150.981		
14	C2/m	4	14.361	4.007	8.781	126.306	95 (6)	4 (fix)
20.1	C2/c	4	9.692	6.737	7.574	116.181	125.3 (1.6)	4 (fix)
BST-0.9								
ambient	R-3m	3	4.272	4.272	30.390	160.701	29.1 (2.0)	8.7 (1.2)
0.5	R-3m	3	4.260	4.260	30.264	158.551		
12.5	C2/m	4	14.319	3.974	8.879	126.269	69 (8)	4 (fix)
19.9	C2/c	4	9.749	6.738	7.440	114.632	147 (11)	4 (fix)

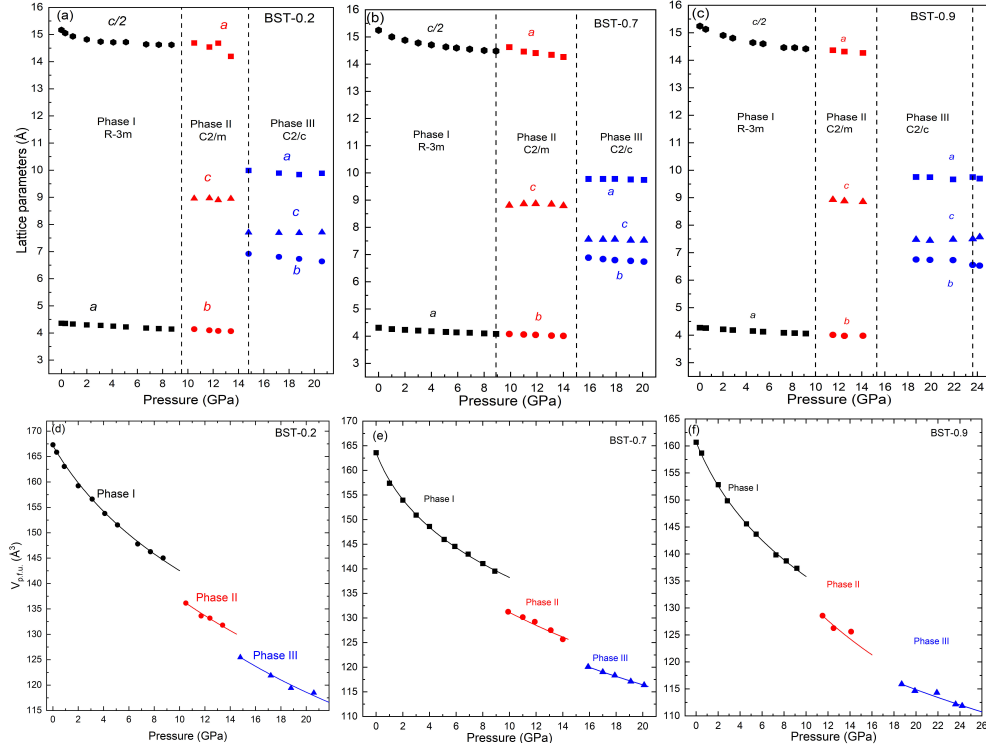


Fig. 3 Pressure dependence of the lattice parameters and cell volume per formula unit of (a),(d) BST-0.2, (b),(e) BST-0.7 and (c),(f) BST-0.9 as a function of pressure. The vertical dashed line indicates the critical pressures of the phase transitions.

3.1.2 X-ray Diffraction of BST-0.7 up to Mbar pressures

Aiming to explore the pressure stability range of the disordered solid-solution BCC phase, BST-0.7 was pressurized up to 180 GPa. Part of our motivation was to explore the effect of solid-solution, as opposed to the ordered B2 CsCl-type phase, to the pressure stability of the BCC phase. The B2 phase of NaCl remains stable up to ≥ 300 GPa [32, 33], while it is predicted to transform to an orthorhombic oC8 phase above 325 GPa [34]. On the other hand, the much heavier elements CsI, that adopts the CsCl-type structure under ambient conditions, has been reported to transform to an orthorhombic structure already at 45 GPa, and finally transform to an HCP-like structure at higher pressures [35, 36].

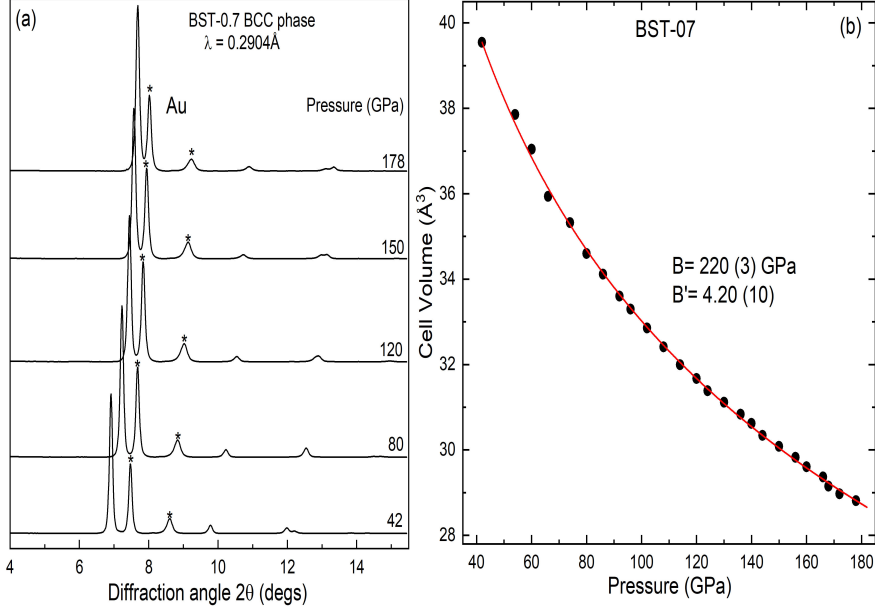


Fig. 4 (a) XRD patterns of BST-0.7 at selected pressures up to 178 GPa. The asterisks denote the Bragg peaks from Au (pressure marker). (b) Pressure dependence of the BCC cell volume of BST-0.7. The red solid curve is a 3rd order Birch-Murnaghan EOS [31] fitted to the experimental data. The determined bulk moduli at the onset pressure are also given.

The XRD results of this study indicate that BST-0.7 remains in the BCC phase up to, at least, 180 GPa, see Fig. 4. For comparison, from previous studies it has been established that Bi remains in the BCC phase up to at least 220 GPa [37]. On the other hand, the BCC phase of Te transforms to the FCC phase at 99 GPa, and the FCC phase remains stable up to, at least, 330 GPa [38]. Finally, Sb adopts a BCC structure at 28 GPa, that remain stable up to 43 GPa [39]. According to Ref. [17], pressure results to a substantial Bi→Te charge transfers, resulting in an enhanced HP ionicity of the BCC phase of Bi₂Te₃. Thus, the extended stability of the BCC phase could presumably be attributed to this enhanced ionicity that stabilizes the BCC phase. A

similar scenario was determined for the extended stability of the α -Mn phase, above the pressure that the HCP phase becomes energetically favorable [40].

3.2 Electrical measurements

The electrical resistance of BST-0.7 as a function of pressure, at room temperature, is shown in Fig. 5(a), for both the compression and decompression runs. Our main motivation for studying the electrical properties of BST-0.7 under pressure was our observation that, at ambient pressure, BST-0.7 shows an almost temperature-independent conductivity, in contrast to the clear semiconducting and metallic behavior of BST-0 (Bi_2Te_3) and BST-1 (Sb_2Te_3), respectively, see Fig. S4 [41]. Upon initial compression, the resistance rapidly decreases, reaching an almost constant value above ≈ 11 -12 GPa. Such a pressure-dependent behavior of the resistance is attributed to a pressure-induced semiconductor to metal transition [42]. A similar pressure dependence of the electrical resistivity was also observed in the case of pure Bi_2Te_3 [43]. Upon decompression, the resistance starts to increase around 6 GPa, and reaches almost the same, with initial compression, value at near ambient pressure with a hysteresis of ≈ 5 -6 GPa.

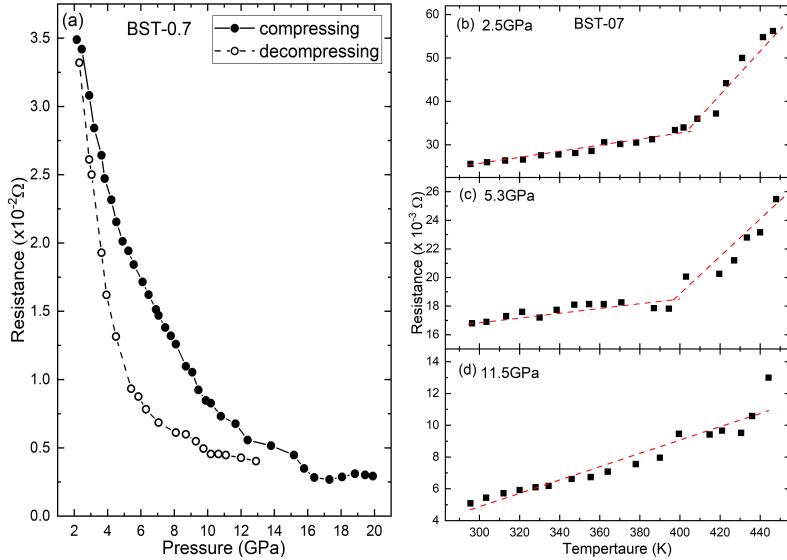


Fig. 5 (a) Electrical resistance of BST-0.7 as a function of pressure, at room temperature, under compression (solid symbols) and decompression (open symbols). Electrical resistance of BST-0.7 as a function of temperature at (b) 2.5 GPa, (c) 5.3 GPa and (d) 11.5 GPa. The dashed red lines are guides to the eye, see text for details.

To confirm the pressure-induced metallization, we performed high-temperature electrical measurements at different pressures, see Figs. 5(b)-(d). We note that, because of different experimental runs, and the fact that resistance is not an intrinsic property

of the sample, comparison between absolute resistance values between runs is challenging. However, the temperature dependence of the resistance (metallic character) is of major importance. At 2.5 and 5.3 GPa, the resistance remains practically constant up to a certain temperature, indicative of a material with very narrow band-gap, and then linearly increases with temperature, thus showing a clear metallic character. On the other hand, at 11.5 GPa, the resistance increases monotonically with temperature, highlighting the metallic character of the material at this pressure from room temperature. We note that, although challenging to establish a definite crossover temperature, the transition from narrow-band-gap \rightarrow metallic character appears to occur at lower T for 5.3 GPa than 2.5 GPa; see dashed red lines in Figs. 5(b) and (c).

4 Discussion

4.0.1 Pressure dependence of the c/a axial ratio in the ambient phase of BST- x

In previous high-pressure studies of the ambient phase of Bi_2Te_3 , a crossover of the pressure dependence of the c/a axial ratio was observed [44, 45]. In details, c/a initially decreases, as expected based on weaker van der Waals interlayer (c -axis) bonding, followed by an increase above 2.5-3.5 GPa. Polian *et al.* [44], attributed this trend to an electronic topological transition (ETT), that mainly affects the intralayer electronic distribution of the strong ionocovalent bonds, rendering a -axis more compressible. The same crossover behavior of the c/a ratio was observed for all the BST compounds in this study, see Fig. 6. Although determination of the exact crossover pressure is challenging, no clear trend was observed with varying Sb concentration. Thus, we conclude that the appearance of the EET is universal for BST compounds and independent of the Sb concentration.

4.0.2 Effect of the Sb concentration on the critical pressure for the formation of the solid-solution BCC phase

The structural analysis of the BST compounds in this study clearly indicates the critical pressure for the formation of the BCC phase increases with increasing Sb concentration. In detail, for BST-0.2 the first sign for the appearance of the BCC phase is at 17.2 GPa, no BCC phase was observed for BST-0.7 up to 20 GPa, and for BST-0.9 BCC appears at 23.6 GPa, see Figs. 1 and 2. The observed trend is in agreement with that reported for pure Bi_2Te_3 (BST-0) [17, 18] and the corresponding observation of the BCC phase above 14.5 GPa. A previous study on Sb_2Te_3 , with the appearance of BCC phase above 21.6 GPa [19], seems to contradict this trend. However, this apparent disagreement can be resolved considering that in Ref. [19], a 4:1 methanol-ethanol mixture was used as PTM, that is heavily non-hydrostatic above 12 GPa [24]. It is well known that non-hydrostatic conditions promote phase transitions to occur at lower pressures [46]. A similar trend could also be claimed for the formation of the $C2/c$ phase, see Fig.2. However, the relatively small pressure differences and experimental limitations preclude a conclusion about a definite trend.

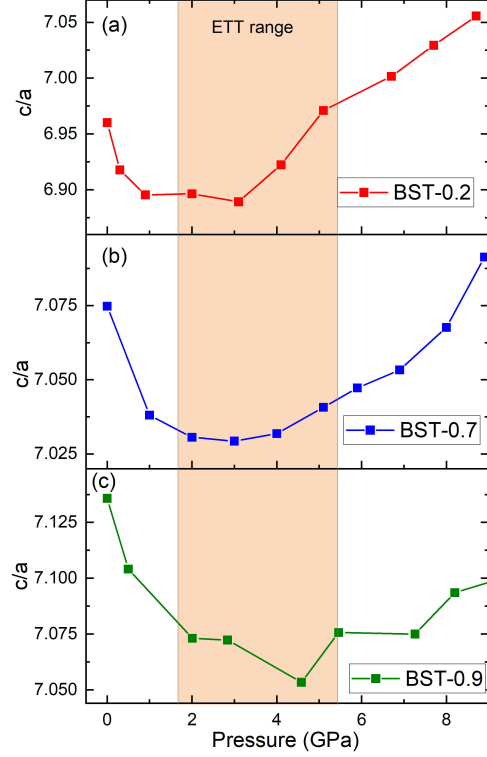


Fig. 6 c/a ratios of the $R - 3m$ phase of a) BST-0.2, b) BST-0.7 and c) BST-0.9 as function of pressure. The orange rectangle denotes the range of the EET transition, see text. The solid lines are guides for the eye.

The trend discussed above, of increasing critical pressure for the formation of a solid-solution BCC phase upon increasing the Sb concentration, appears to be counterintuitive. Under ambient conditions, the atomic radius of Sb is closer (than that of Bi) to Te, and according to theoretical calculations, this continues to be valid under pressure [47, 48]. Thus, and having in mind the Hume-Rothery rule that solid-solutions are promoted when atomic radii are close, the opposite effect shall be expected. To conclude, the underlying reason for the observed trend is still not well understood, and further studies, presumably theoretical, are needed to elucidate this effect.

4.0.3 Electrical properties under pressure

As mentioned in the results section, the transition from narrow-band-gap \rightarrow metallic character appears to occur at lower T upon pressure increase. This is in agreement with the general intuition that pressure promotes metallic character. Moreover, previous density functional theory (DFT) calculations [4] for the ambient conditions $R - 3m$ phase of Bi_2Te_3 , document that application of compressive strain along the c -axis results to an abrupt decrease of the band gap, eventually reaching metallization at $\approx 12\%$ compressive strain. Although a direct comparison with the present results under

hydrostatic pressure is not possible, BST-0.7 undergoes a phase transition when the c -axis relative compression becomes higher than $\approx 5\%$ (see Fig. 3(b)) at ≈ 9 GPa, a common trend can be inferred. Nevertheless, the previous DFT calculations and present results do agree on the rapid decrease of the band gap under compression.

Finally, we note that although attributing the crossover of the pressure dependence of the c/a axial ratio to an EET transition looks reasonable, from our electrical measurements no direct effect on the electrical conductivity as a function of pressure was observed at the relevant pressure range. Indeed, the electrical conductivity shows a smooth variation between 2-8 GPa.

5 Conclusions

All the BST- x compounds ($x=0.2, 0.7$ and 0.9) investigated in this study exhibit identical structural evolution under pressure, that is also identical with the one for pure Bi_2Te_3 and Sb_2Te_3 . Sb concentration marginally, if at all, affects critical pressures for the phase I \rightarrow phase II \rightarrow phase III phase transitions. However, increasing Sb concentration results to a clear increase of the critical pressure for the transition to the disordered BCC phase IV. The exact origin of this effect is still not clear. In the case of BST-0.7, the BCC phase was found to have an extensive pressure stability up to 180 GPa. For the same BST alloy, a pressure induced metallization was observed above 12 GPa. Finally, a clear crossover of the value of the c/a axial ratio of the ambient phase with increasing pressure, previously attributed to a pressure-induced EET transition, was observed for all BST compounds of this study.

Supplementary information. Supplementary Figs. 1-4 are provided in Supplementary information file.

Acknowledgements. C.W. and S.F. acknowledge support from the Graduate Scholarships of the Guangdong Provincial Key Laboratory of Materials and Technologies for Energy Conversion. Y.A. would like to acknowledge generous support from the Pazy Research Foundation, Grant No. 2032063. The work performed at GTIIT was supported by funding from the Guangdong Technion Israel Institute of Technology and the Guangdong Provincial Key Laboratory of Materials and Technologies for Energy Conversion, MATEC (No. MATEC2022KF001). Beamline 12.2.2 at the Advanced Light Source is a DOE Office of Science User Facility under contract no. DE-AC02-05CH11231. Part of the synchrotron radiation experiments were performed at BL10XU of SPring-8 with the approval of the Japan Synchrotron Radiation Research Institute (JASRI) (Proposal Nos. 2024A1096 and 2024B1182). We also acknowledge DESY (Hamburg, Germany), a member of the Helmholtz Association HGF, for the provision of experimental facilities. Parts of this research were carried out at PETRA III beamline P02.2.

Conflict of Interest

The authors have no conflicts to disclose.

Data Availability

The data that support the findings of this study are available from the corresponding author upon reasonable request.

References

- [1] H. Mansouri, S. A. Sajjadi, A. Babakhani, and Y. Saberi, Microstructure and thermoelectric performance evaluation of p-type $(\text{Bi}, \text{Sb})_2\text{Te}_3$ materials synthesized using mechanical alloying and spark plasma sintering process, *J. Mater. Sci.: Mater. Electron.* **32**, 9858 (2021).
- [2] Y. Sun, H. Qin, C. Zhang, H. Wu, L. Yin, Z. Liu, S. Guo, Q. Zhang, W. Cai, H. Wu, F. Guo, and J. Sui, Sb_2Te_3 based alloy with high thermoelectric and mechanical performance for low-temperature energy harvesting, *Nano Energy* **107**, 108176 (2023).
- [3] G. D. Mahan, Good Thermoelectrics, in *Solid State Physics*, Solid State Physics, Vol. 51, edited by H. Ehrenreich and F. Spaepen (Academic Press, 1998) pp. 81–157.
- [4] C. Gayner, Y. Natanzon, Y. Kauffmann, and Y. Amouyal, Topologically-enhanced thermoelectric properties in Bi_2Te_3 -based compounds: Effects of grain size and misorientation, *ACS Appl. Mater. Interfaces* **14**, 49730 (2022).
- [5] M. K. Jacobsen, R. S. Kumar, A. L. Cornelius, S. V. Sinogeiken, and M. F. Nico, High pressure x-ray diffraction studies of $\text{Bi}_{2-x}\text{Sb}_x\text{Te}_3$ ($x = 0,1,2$), *AIP Conf. Proc.* **955**, 171 (2007).
- [6] F. J. Manjón, R. Vilaplana, O. Gomis, E. Pérez-González, D. Santamaría-Pérez, V. Marín-Borrás, A. Segura, J. González, P. Rodríguez-Hernández, A. Muñoz, C. Drasar, V. Kucek, and V. Muñoz-Sanjosé, High-pressure studies of topological insulators Bi_2Se_3 , Bi_2Te_3 , and Sb_2Te_3 , *Phys. Status Solidi B* **250**, 669 (2013).
- [7] Y. Feutelais, B. Legendre, N. Rodier, and V. Agafonov, A study of the phases in the bismuth - tellurium system, *Mater. Res. Bull.* **28**, 591 (1993).
- [8] S. Nakajima, The crystal structure of $\text{Bi}_2\text{Te}_{3-x}\text{Se}_x$, *J. Phys. Chem. Solids* **24**, 479 (1963).
- [9] Y. Hosokawa, K. Tomita, and M. Takashiri, Growth of single-crystalline Bi_2Te_3 hexagonal nanoplates with and without single nanopores during temperature-controlled solvothermal synthesis, *Sci. Rep.* **9**, 10790 (2019).
- [10] S. V. Ovsyannikov, V. V. Shchennikov, G. V. Vorontsov, A. Y. Manakov, A. Y. Likhacheva, and V. A. Kulbachinskii, Giant improvement of thermoelectric power factor of Bi_2Te_3 under pressure, *J Appl. Phys.* **104**, 053713 (2008).

- [11] L. G. Khvostantsev, A. I. Orlov, N. Kh. Abrikosov, T. E. Svechnikova, and S. N. Chizhevskaya, Thermoelectric properties and phase transitions in Bi_2Te_3 under hydrostatic pressure up to 9 GPa and temperature up to 300 C, *Phys. Status Solidi A* **71**, 49 (1982).
- [12] M. K. Jacobsen, S. V. Sinogeikin, R. S. Kumar, and A. L. Cornelius, High pressure transport characteristics of Bi_2Te_3 , Sb_2Te_3 , and BiSbTe_3 , *J. Phys. Chem. Solids* **73**, 1154 (2012).
- [13] M. Il'ina and E. Itskevich, Superconductivity of bismuth telluride at high pressure, *Fiz Tverd Tela+ Sverkhprovodimost' tellurida vismuta pod vysokim davleniem*, **17**, 154 (1975).
- [14] J. Zhu, J. L. Zhang, P. P. Kong, S. J. Zhang, X. H. Yu, J. L. Zhu, Q. Q. Liu, X. Li, R. C. Yu, R. Ahuja, W. G. Yang, G. Y. Shen, H. K. Mao, H. M. Weng, X. Dai, Z. Fang, Y. S. Zhao, and C. Q. Jin, Superconductivity in Topological Insulator Sb_2Te_3 Induced by Pressure, *Sci. Rep.* **3**, 2016 (2013).
- [15] S. J. Zhang, J. L. Zhang, X. H. Yu, J. Zhu, P. P. Kong, S. M. Feng, Q. Q. Liu, L. X. Yang, X. C. Wang, L. Z. Cao, W. G. Yang, L. Wang, H. K. Mao, Y. S. Zhao, H. Z. Liu, X. Dai, Z. Fang, S. C. Zhang, and C. Q. Jin, The comprehensive phase evolution for Bi_2Te_3 topological compound as function of pressure, *Journal of Applied Physics* **111**, 112630 (2012).
- [16] M. Einaga, Y. Tanabe, A. Nakayama, A. Ohmura, F. Ishikawa, and Y. Yamada, New superconducting phase of Bi_2Te_3 under pressure above 11 GPa, *J. Phys.: Conf. Ser.* **215**, 012036 (2010).
- [17] L. Zhu, H. Wang, Y. Wang, J. Lv, Y. Ma, Q. Cui, Y. Ma, and G. Zou, Substitutional Alloy of Bi and Te at High Pressure, *Phys. Rev. Lett.* **106**, 145501 (2011).
- [18] M. Einaga, A. Ohmura, A. Nakayama, F. Ishikawa, Y. Yamada, and S. Nakano, Pressure-induced phase transition of Bi_2Te_3 to a bcc structure, *Phys. Rev. B* **83**, 092102 (2011).
- [19] Y. Ma, G. Liu, P. Zhu, H. Wang, X. Wang, Q. Cui, J. Liu, and Y. Ma, Determinations of the high-pressure crystal structures of Sb_2Te_3 , *J. Phys.: Condens. Matter* **24**, 475403 (2012).
- [20] S. M. Souza, C. M. Poffo, D. M. Trichês, J. C. de Lima, T. A. Grandi, A. Polian, and M. Gauthier, High pressure monoclinic phases of Sb_2Te_3 , *Phys. B: Condens. Matter* **407**, 3781 (2012).
- [21] F.-X. Bai, H. Yu, Y.-K. Peng, S. Li, L. Yin, G. Huang, L.-C. Chen, A. F. Goncharov, J.-H. Sui, and F. Cao, Electronic topological transition as a route to improve thermoelectric performance in $\text{Bi}_{0.5}\text{Sb}_{1.5}\text{Te}_3$, *Adv. Sci.* **9**, 2105709 (2022).

- [22] K. Syassen, Ruby under pressure, [High Pressure Res.](#) **28**, 75 (2008).
- [23] O. L. Anderson, D. G. Isaak, and S. Yamamoto, Anharmonicity and the equation of state for gold, [J. Appl. Phys.](#) **65**, 1534 (1989).
- [24] S. Klotz, J.-C. Chervin, P. Munsch, and G. Le Marchand, Hydrostatic limits of 11 pressure transmitting media, [J. Phys. D: Appl. Phys.](#) **42**, 075413 (2009).
- [25] M. Kunz, A. A. MacDowell, W. A. Caldwell, D. Cambie, R. S. Celestre, E. E. Domning, R. M. Duarte, A. E. Gleason, J. M. Glossinger, and N. Kelez, A beamline for high-pressure studies at the Advanced Light Source with a superconducting bending magnet as the source, [J. Synchrotron Radiat.](#) **12**, 650 (2005).
- [26] S. Kawaguchi-Imada, R. Sinmyo, K. Ohta, S. Kawaguchi, and T. Kobayashi, Submillisecond in situ X-ray diffraction measurement system with changing temperature and pressure using diamond anvil cells at BL10XU/SPring-8, [J. Synchrotron Radiat.](#) **31**, 343 (2024).
- [27] C. Prescher and V. B. Prakapenka, DIOPTAS: a program for reduction of two-dimensional X-ray diffraction data and data exploration, [High Pressure Research](#) **35**, 223 (2015).
- [28] W. Kraus and G. Nolze, POWDER CELL—a program for the representation and manipulation of crystal structures and calculation of the resulting X-ray powder patterns, [J. Appl. Crystallogr.](#) **29**, 301 (1996).
- [29] A. Boultif and D. Louër, Powder pattern indexing with the dichotomy method, [J. Appl. Crystallogr.](#) **37**, 724 (2004).
- [30] B. H. Toby and R. B. Von Dreele, GSAS-II: the genesis of a modern open-source all purpose crystallography software package, [J. Appl. Crystallogr.](#) **46**, 544 (2013).
- [31] F. Birch, Finite strain isotherm and velocities for single-crystal and polycrystalline NaCl at high pressures and 300°k, [Journal of Geophysical Research: Solid Earth](#) **83**, 1257 (1978).
- [32] S. Ono, The equation of state of B2-type NaCl, [Journal of Physics: Conference Series](#) **215**, 012196 (2010).
- [33] T. Sakai, E. Ohtani, N. Hirao, and Y. Ohishi, Equation of state of the NaCl-B2 phase up to 304 GPa, [Journal of Applied Physics](#) **109**, 084912 (2011).
- [34] X. Chen and Y. Ma, High-pressure structures and metallization of sodium chloride, [Europhysics Letters](#) **100**, 26005 (2012).
- [35] H. K. Mao, R. J. Hemley, L. C. Chen, J. F. Shu, L. W. Finger, and Y. Wu, X-ray diffraction to 302 Gigapascals: High-pressure crystal structure of Cesium Iodide,

Science **246**, 649 (1989).

- [36] H. K. Mao, Y. Wu, R. J. Hemley, L. C. Chen, J. F. Shu, L. W. Finger, and D. E. Cox, High-pressure phase transition and equation of state of CsI, *Phys. Rev. Lett.* **64**, 1749 (1990).
- [37] Y. Akahama, H. Kawamura, and A. K. Singh, Equation of state of bismuth to 222 GPa and comparison of gold and platinum pressure scales to 145 GPa, *J. Appl. Phys.* **92**, 5892 (2002).
- [38] Y. Akahama, N. Okawa, T. Sugimoto, H. Fujihisa, N. Hirao, and Y. Ohishi, Coexistence of a metastable double hcp phase in bcc-fcc structure transition of Te under high pressure, *Jpn. J. Appl. Phys.* **57**, 025601 (2018).
- [39] O. Degtyareva, M. I. MCMahon, and R. J. Nelmes, High-pressure structural studies of group-15 elements, *High Pressure Research* **24**, 319 (2004).
- [40] L. K. Magad-Weiss, A. A. Adeleke, E. Greenberg, V. B. Prakapenka, Y. Yao, and E. Stavrou, High-pressure structural study of α -mn: Experiments and calculations, *Phys. Rev. B* **103**, 014101 (2021).
- [41] D. Muhamed, Y. Amoyla, and *et al.*, To be submitted.
- [42] W. Lu, L. Zhang, C. Wei, Q. Zhang, M. Kunz, S. Kawaguchi, H. Kadobayashi, C. Boussard-Plédel, B. Bureau, J. Jiang, A. S. Ahmad, Y. Ein-Eli, and E. Stavrou, Pressure-induced crystallization and metallization in glassy As₂₀Se₈₀, *Phys. Rev. B* **111**, 024115 (2025).
- [43] J. Zhang, C. Liu, X. Zhang, F. Ke, Y. Han, G. Peng, Y. Ma, and C. Gao, Electronic topological transition and semiconductor-to-metal conversion of Bi₂Te₃ under high pressure, *Applied Physics Letters* **103**, 052102 (2013).
- [44] A. Polian, M. Gauthier, S. M. Souza, D. M. Trichês, J. a. Cardoso de Lima, and T. A. Grandi, Two-dimensional pressure-induced electronic topological transition in Bi₂Te₃, *Phys. Rev. B* **83**, 113106 (2011).
- [45] A. Nakayama, M. Einaga, Y. Tanabe, S. Nakano, F. Ishikawa, and Y. Yamada, Structural phase transition in Bi₂Te₃ under high pressure, *High Pressure Res.* **29**, 245 (2009).
- [46] X. Zhang, L. Dai, H. Hu, M. Hong, and C. Li, Pressure-induced reversible structural phase transitions and metallization in GeTe under hydrostatic and non-hydrostatic environments up to 22.9 GPa, *J. Non-Cryst. Solids* **618**, 122516 (2023).
- [47] M. Rahm, R. Hoffmann, and N. W. Ashcroft, Atomic and ionic radii of elements 1–96, *Chemistry – A European Journal* **22**, 14625 (2016).

- [48] M. Rahm, M. Ångqvist, J. M. Rahm, P. Erhart, and R. Cammi, Non-bonded radii of the atoms under compression, [ChemPhysChem](#) **21**, 2441 (2020).